1.E.1:
2.B

Nuclear Physics **A344** (1980) 15–40;

STRONG COUPLED-CHANNELS EFFECTS IN THE ^{9}Be(α, t)^{10}B REACTION

M. N. HARAKEH, J. VAN POPTA, A. SAHA and R. H. SIEMSSEN

Kernfysisch Versneller Instituut, Groningen, The Netherlands

Received 14 January 1980
(Revised 24 March 1980)

Abstract: Differential cross sections were measured for the reactions ^{9}Be(α, α′)^{9}Be, ^{9}Be(α, t)^{10}B and ^{9}Be(α, ^{3}He)^{10}B at $E_{\alpha} = 65$ MeV for angles ranging from $\theta_{lab} = 6°$ to 48°. Optical-model analysis was performed for elastic α-scattering from ^{9}Be at $E_{\alpha} = 48$, 65 and 104 MeV, and DWBA and CC calculations were done for the inelastic α-scattering at $E_{\alpha} = 65$ MeV. DWBA calculations for the ^{9}Be(α, ^{3}He) reactions do not fit the transfer data so well and extracted spectroscopic factors are in disagreement with those of Cohen and Kurath and with values obtained from other reactions. Full CRC calculations assuming a band structure for the low-lying states of ^{10}B and employing a modified set of Cohen and Kurath spectroscopic factors yield globally better fits both in shape and in absolute cross section for differential cross sections to low-lying states in ^{10}B obtained in ^{9}Be(α, t)^{10}B at $E_{\alpha} = 65$ MeV and ^{9}Be(^{3}He, d)^{10}B at $E_{d} = 17$ MeV. In general, strong coupled-channel effects mainly affecting the distorted waves are observed both in entrance and exit channels.

E | NUCLEAR REACTIONS ^{9}Be(α, α′), (α, t), (α, ^{3}He), $E = 65$ MeV; measured $\sigma(E_{\alpha}, \theta)$; deduced optical-model parameters; measured $\sigma(E_{t}, \theta)$, $\sigma(E_{^{3}He}, \theta)$. ^{9}Be levels deduced β_2. ^{10}B, ^{10}Be levels deduced l, S. DWBA, coupled-channel analyses. Natural target.

1. Introduction

Anomalies in proton transfer reactions with ^{9}Be as target have been known for a long time. A discrepancy exists between the (^{3}He, d) and the (d, n) spectroscopic factors for the first $T = 1$ state in ^{10}B if the conventional DWBA is employed [1,2]). This discrepancy is at least partially removed if the analysis is generalised so as to include isospin and charge exchange [3,4]).

An anomaly of apparently different nature is observed for the ^{9}Be (α, t) reaction. Whereas in the (d, n) and the (^{3}He, d) reactions the first excited state ($J^{\pi} = 1^{+}$, $T = 0$) at 0.72 MeV in ^{10}B is excited with about the same strength as the ($J^{\pi} = 3^{+}$, $T = 0$) ground state of ^{10}B, the relative strength of the first excited state is by about a factor of two weaker in the ^{9}Be(α, t)^{10}B reaction [5]). This is schematically shown in fig. 1. The discrepancies between the different proton transfer reactions are the more striking as they occur in the relative spectroscopic factors of transitions that do not differ much in Q-value (for the same reaction type) and that involve large spectros-

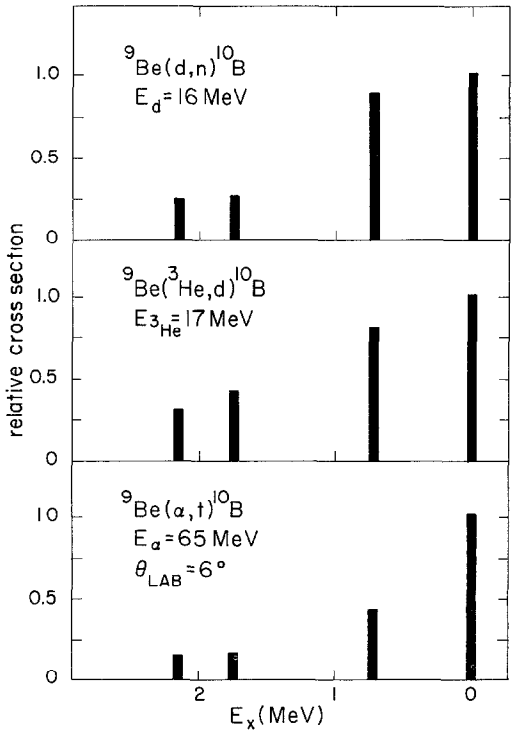

Fig. 1. Relative cross sections at the first maxima for the lowest four states in ^{10}B as observed in the $^{9}Be(d, n)$ reaction at E_d = 16 MeV and $^{9}Be(^{3}He, d)$ reaction at $E_{^3He}$ = 17 MeV and at 6° in the $^{9}Be(\alpha, t)$ reaction at E_α = 65 MeV.

copic factors and the same *l*-transfers, at least if one does not invoke f-state admixtures.

Several possible explanations for the g.s., first excited state discrepancy have been suggested [4-6]: A strong forward-angle *j*-dependence of the (α, t) reaction (the g.s. transition is $p_{\frac{3}{2}}$, the transition to the first excited state predominantly $p_{\frac{1}{2}}$), an f-state admixture in ^{10}B, and coupled-channels effects. Since the (α, t) reaction is strongly momentum mismatched, small f-state admixtures may lead to sizeable effects. The g.s. transition ($\frac{3}{2}^- \rightarrow 3^+$) could involve both $f_{\frac{5}{2}}$ and $f_{\frac{7}{2}}$ transfers, whereas $f_{\frac{5}{2}}$ transfer only is allowed for the first excited state ($\frac{3}{2}^- \rightarrow 1^+$). In one analysis [4]) f-state admixtures were found to lead to somewhat improved fits to the g.s. (α, t) angular distributions, but they did not resolve the discrepancies in the relative cross sections. Coupled-channels calculations for the ^{9}Be $(\alpha, t)^{10}B$ reaction up to now have been performed only on a limited scale. These also did not resolve the discrepancy [4]).

Yet another anomaly was found by Kemper *et al.* [4]) in a study of the ^{9}Be and $^{13}C(\alpha, t)$ reactions at E_α = 27 MeV in which the transition to the 0^+, $T = 1$ states were suppressed by at least a factor of five, compared to the transitions to the $T = 0$

states. The latter anomaly seems to be related to the relatively low bombarding energy and the strong angular momentum mismatch of the (α, t) reaction, since it is absent at $E_\alpha = 43$ MeV [refs. [5,6])] and at 65 MeV at which the present study is done.

Since the angular momentum mismatch decreases with increasing bombarding energy we have studied the ^{9}Be (α, t) and (α, ^{3}He) reactions at $E_\alpha = 65$ MeV, which is about the maximum energy at which tritons could still be stopped with our detector telescope. The data have been subjected to very extensive coupled-channels calculations (CC and CRC). We find that the discrepancy between the (^{3}He, d) and the (α, t) relative spectroscopic factors for the g.s. and the first excited state can be explained by coupled-channels effects that are more important for the angular momentum mismatched (α, t) reaction than for the matched (^{3}He, d) reaction. In addition we have obtained new spectroscopic information for ^{10}Be from the ^{9}Be (α, ^{3}He) ^{10}Be reaction. This will be discussed together with the ^{9}Be (α, t) spectroscopic data. For the discussion of the reaction mechanism we mainly concentrate on the ^{9}Be (α, t) reaction leading to the ground state and the first three excited states in ^{10}B, and on the ^{9}Be+α elastic and inelastic scattering.

2. Experimental procedure and results

A momentum-analysed beam of 65 MeV α-particles was obtained from the KVI isochronous, energy variable cyclotron. The target consisted of a self-supporting foil of metallic beryllium rolled to a thickness of 0.69 mg/cm^2. Reaction products were detected with a telescope consisting of a 0.4 mm thick ΔE and a 5 mm thick E surface barrier detector. The solid angle of the aperture was 0.133 msr, and the

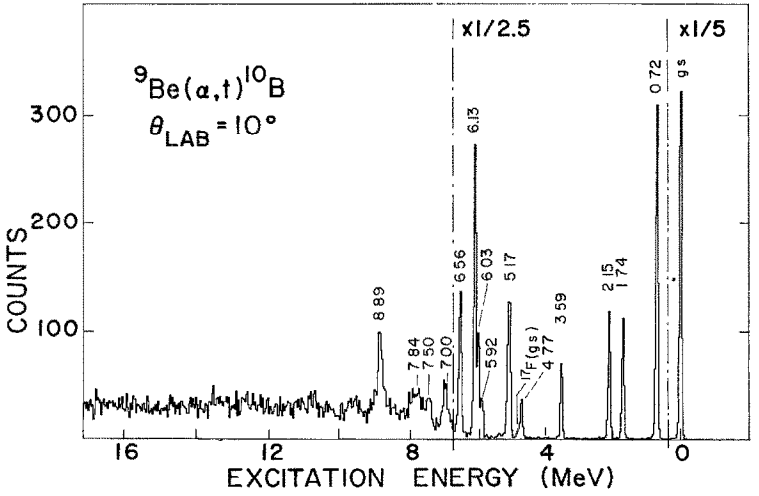

Fig. 2. A ^{9}Be(α, t)^{10}B spectrum taken at $\theta_{lab} = 10°$. ^{10}B peaks are labelled with their excitation energies. Contaminant fluorine peak is indicated.

angular acceptance 0.3°. Data acquisition and software particle identification was performed on a PDP-15 computer with the program SOFBAL [7]).

Spectra were measured at 22 angles from 6° to 48° in the laboratory system. Typical spectra from the (α, t) and the (α, ^{3}He) reactions are shown in figs. 2 and 3. The energy resolution was about 80 keV at forward angles and it increased with increasing angle due to kinematic broadening. Elastic and inelastic α-scattering cross sections

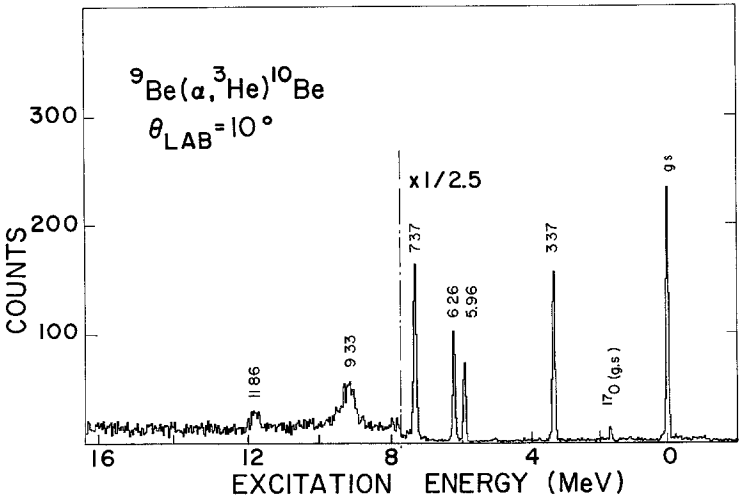

Fig. 3. A $^{9}Be(\alpha, t)^{10}Be$ spectrum taken at $\theta_{lab} = 10°$. ^{10}Be peaks are labelled with their excitation energies. Contaminant oxygen peak is indicated.

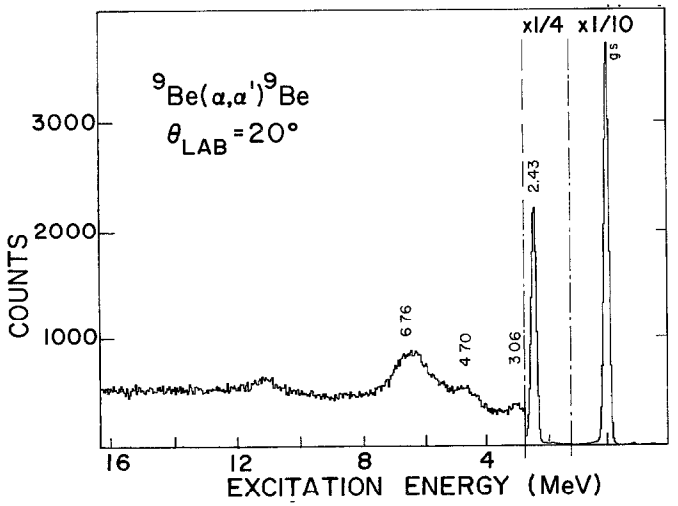

Fig. 4. A $^{9}Be(\alpha, \alpha)^{9}Be$ spectrum taken at $\theta_{lab} = 20°$. Some ^{9}Be states excited in this reaction are labelled with their excitation energies.

were measured simultaneously. The $\frac{5}{2}^-$ state at 2.43 MeV and $\frac{7}{2}^-$ state at 6.76 MeV belonging to the $\frac{3}{2}^-$ ground-state band of ^{9}Be are clearly observed in the ^{9}Be (α, α') ^{9}Be spectrum shown in fig. 4. Absolute cross sections were obtained by normalizing the inelastic and reaction data to the ^{9}Be+α elastic scattering that in turn was normalized to optical-model predictions at forward angles. The target thickness deduced by this method agrees within 15 % with the thickness derived from the differential energy loss of α-particles from a radioactive source after passing through the foil. The absolute cross sections are estimated to be accurate to 15 %.

3. Optical-model and DWBA analysis

3.1. ELASTIC AND INELASTIC SCATTERING

Optical-model calculations were performed with the code OPTIM [8]. Starting parameters for the searches were those of the potentials A48 and B104 that are representative of two different families, where the former was obtained from fitting ^{9}Be+α elastic scattering at $E_\alpha = 48$ MeV [ref. [9])] and the latter from refitting the elastic scattering data [10]) at 104 MeV. The parameters of these

TABLE 1

Optical-model potential parameters used in DWBA and CRC analysis of (α, t) and (^{3}He, d) reactions on ^{9}Be

Channel	Pot.	V (MeV)	r_R (fm)	a_R (fm)	W (MeV)	r_I (fm)	a_I (fm)	r_C (fm)	χ^2_F
$\alpha+^{9}$B	A48 [a])	148.9	1.491	0.587	29.52	1.491	0.587	1.25	
	A65 [b])	146.8	1.491	0.587	35.95	1.491	0.587	1.25	15
	A104 [c])	157.9	1.491	0.587	48.85	1.491	0.587	1.25	49
	B65 [d])	66.4	1.501	0.672	63.5	0.636	1.066	1.25	29
	B104 [e])	67.67	1.501	0.672	73.7	0.636	1.066	1.3	2.8
	A65′ [f])	174.2	1.491	0.587	17.55	1.491	0.587	1.25	37
^{3}He+^{10}Be or t+^{10}B	C [g])	132.9	1.54	0.57	19.5	1.82	0.22	0.81	
^{3}He+^{9}Be	D [h])	152.8	1.202	0.695	29.7	1.22	1.167	1.07	
d+^{10}B	E [i])	73	1.04	0.87	24.0	2.05	0.41	1.3	
P+^{9}Be n+^{9}Be	[j])		1.26	0.60	$\lambda = 20$			1.3	

All potentials are of the Woods-Saxon form; $R = rA_T^{1/3}$, where A_T is the mass of the target nucleus.
[a]) Ref. [9]).
[b]) Obtained by fitting present data with geometrical parameters of A48.
[c]) Obtained by fitting data of ref. [10]) with geometrical parameters of A48.
[d]) Obtained by fitting present data with geometrical parameters of B104.
[e]) Obtained by refitting data of ref. [10]) with all parameters allowed to vary.
[f]) Obtained from CCBA analysis (see text).
[g]) Ref. [9]). [h]) Ref. [9]). [i]) Ref. [20]).
[j]) Adjusted to reproduce binding energy.

potentials are listed in table 1. Quite remarkably both potentials already gave a reasonable good fit to the elastic and inelastic scattering data at $E_\alpha = 65$ MeV without a readjustement of the parameters. As a following step the geometrical parameters were held fixed and a search was performed on V and W. The parameters of the resulting potentials A65 and B65 are given in table 1, and the fits to the data are shown in fig. 5 (solid curves). A subsequent attempt, however, also to fit the

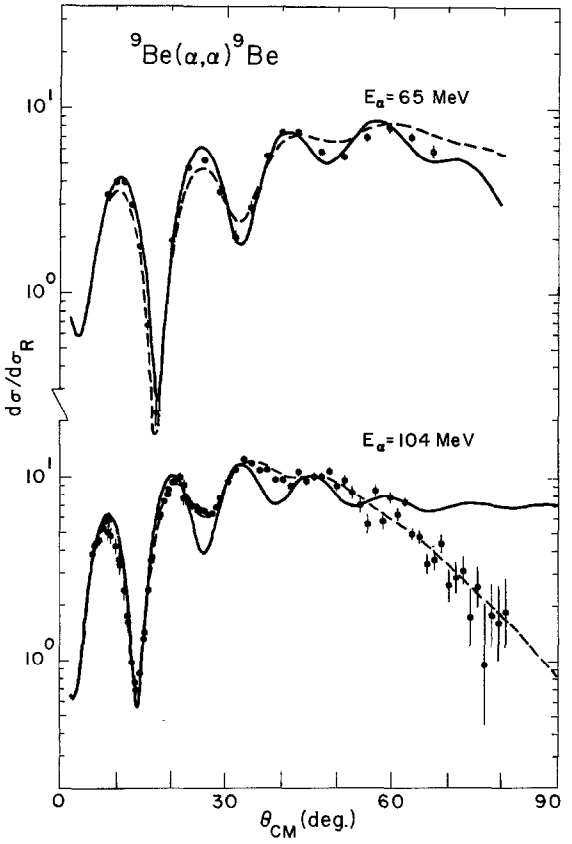

Fig. 5. $^{9}Be(\alpha, \alpha)^{9}Be$ elastic cross sections at $E_\alpha = 65$ MeV (this work) and at $E_\alpha = 104$ MeV [ref. [10])]. Solid and dashed curves are optical model fits with optical model parameters of the A and B families, respectively.

104 MeV data with potential family A yielded (potential A104) significantly poorer fits than potential B104 to the larger angle data (fig. 5).

Inelastic scattering cross sections in the DWBA were calculated with the code DWUCK [11]). In the rotational model the cross section for an odd-A target nucleus is given by the relation

$$\frac{d\sigma}{d\Omega} = \beta^2 |\langle J_i L K 0 | J_f K \rangle|^2 \left(\frac{d\sigma(0 \to I)}{d\Omega}\right)_{DWBA},$$

where β is the deformation parameter, J_i and J_f are the spins of the initial and final states, and K is the quantum number of the rotational band. The Clebsch-Gordan coefficient relates in the strong coupling limit the cross sections in the odd-A nucleus to the $0^+ \rightarrow L^\pi$ transition of the even-A core.

Deformation parameters of 0.68 and 0.66 were found for the transitions to the $\frac{5}{2}^-$ and $\frac{7}{2}^-$ states, respectively, these values being the same for potentials A65 and B65. No additional $L = 4$ contribution was required to fit the data. DWBA fits to the inelastic scattering data are shown in fig. 6 (dashed curves) together with coupled-

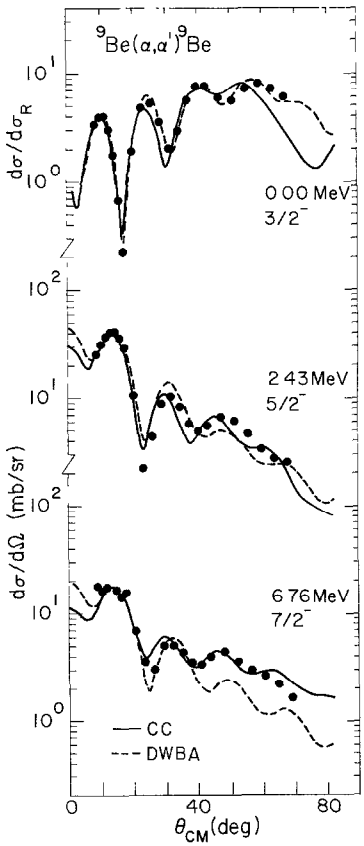

Fig. 6. Elastic and inelasitc cross sections to the $K^\pi = \frac{3}{2}^-$ ground state rotational band of ^{9}Be. Dashed and solid curves are the results of DWBA and CC calculations, respectively. See text for more details.

channels calculations (solid curves) done with the code ECIS. For these coupled channels, reorientation effects have been included. The optical-model parameters for the entrance channel were readjusted so as to maintain a good fit to the elastic scattering data (pot. A65′). A more detailed description of the coupled-channels calculations is given in sect. 4.

3.2. DWBA ANALYSIS OF THE (α, t) AND (α, ^{3}He) REACTION DATA

Zero-range DWBA calculations for the ^{9}Be(α, t)^{10}B and ^{9}Be(α, ^{3}He)^{10}B reactions were performed with the program DWUCK. A finite-range parameter of 0.70 was employed. The optical-model potentials used in these calculations were pot. A65 and pot. C of table 1. The single-particle wave functions were generated in a potential whose geometrical parameters are given in table 1 and whose depth was varied to reproduce the correct binding energy of the single particle. For states unbound to proton or neutron emission in ^{10}B and ^{10}Be, respectively, the single particle was assumed to be slightly bound by 0.1 MeV. Non-locality corrections were ignored for the distorted waves and the bound single particle. The angular distributions

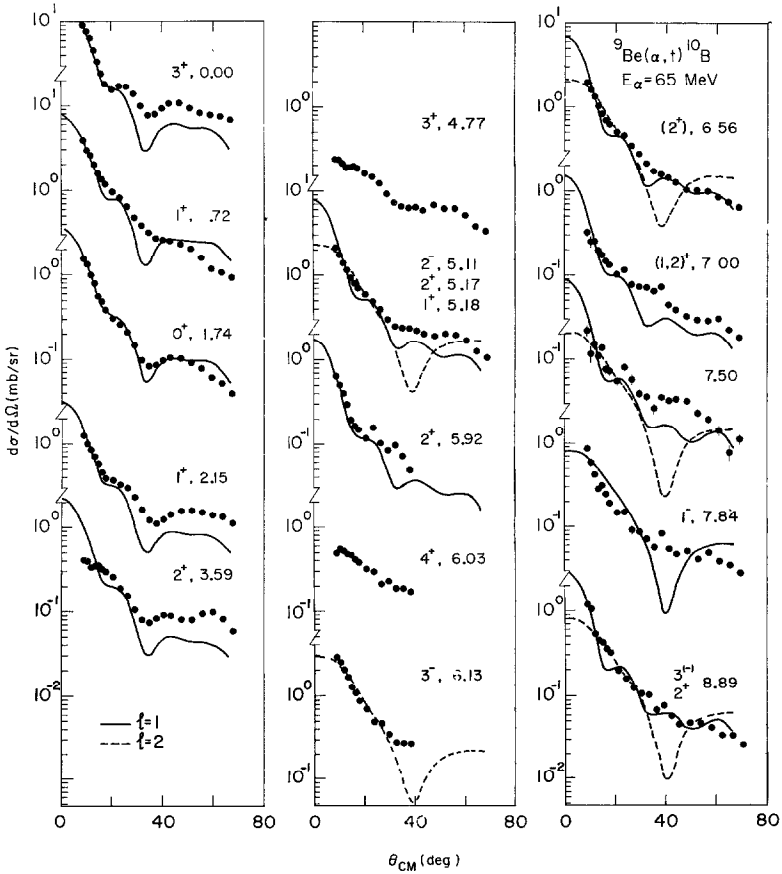

Fig. 7. Differential cross sections for transitions observed in the ^{9}Be(α, t)^{10}B recation. For backward angles, the transitions to the 5.92 MeV, 6.03 MeV and 6.13 MeV states could not be experimentally resolved. Solid and dashed curves are the result of DWBA calculations for $l = 1$ ($1p_{3/2}$) and $l = 2$ ($1d_{5/2}$) transitions, respectively. No DWBA curves are drawn through the states at 4.77 MeV and 6.03 MeV, which are known to be excited mainly by multistep processes.

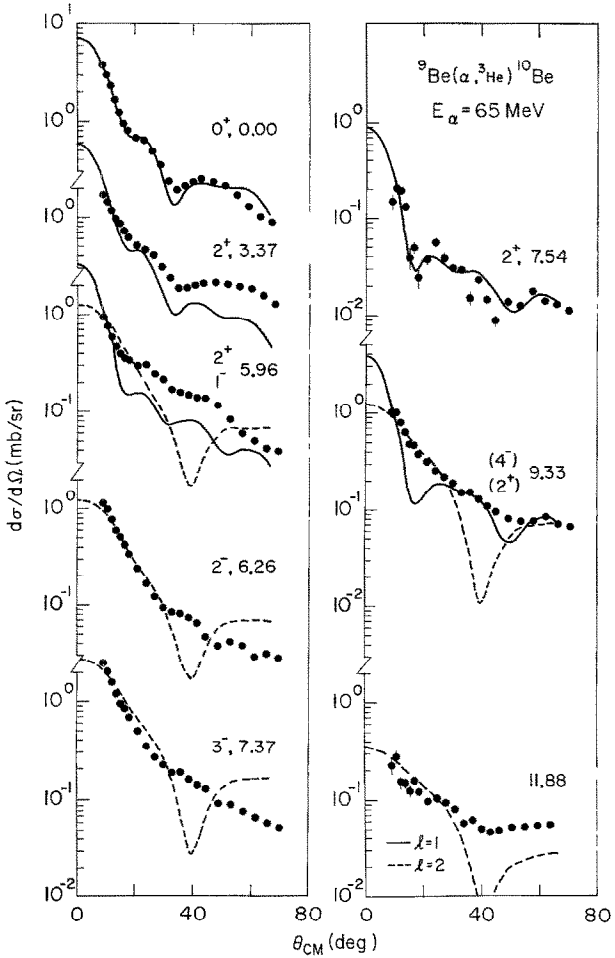

Fig. 8. Differential cross sections for transitions observed in the $^{9}Be(\alpha, ^{3}He)^{10}Be$ reaction. Solid and dashed curves are the results of DWBA calculations for $l = 1$ ($1p_{3/2}$) and $l = 2$ ($1d_{5/2}$) transitions, respectively.

predicted for ^{10}B and ^{10}Be states are shown in figs. 7 and 8, respectively, together with the data. Only in a few cases do the predicted angular distributions fit the data fairly well. In general, the fit is poor except at forward angles for some of the states. The absolute spectroscopic factors were extracted using the relation:

$$\left(\frac{d\sigma}{d\Omega}\right)_{exp} = NC^2S\,\frac{2J_f+1}{(2J_i+1)(2j+1)}\left(\frac{d\sigma}{d\Omega}\right)_{DWUCK},$$

where J_i and J_f are the initial and final state spins; and j is the total angular momentum of the transferred nucleon. A normalization factor $N = 22.6$ was used both for the (α, t) and (α, ^{3}He) reactions. This factor was obtained from the comparison between

TABLE 2

Spectroscopic information for the $^{9}Be(\alpha, t)^{10}B$ reaction as obtained from DWBA analysis

E_x [a] (MeV)	$J^\pi; T$ [a]	l_p [b]	$S(\alpha, t)$ abs.	$S(d, n)$ [c] rel.	$S(^3He, d)$ [d] rel.
0.0	$3^+; 0$	1	0.89	1.0	1.0
0.718	$1^+; 0$	1	1.00	1.97	1.8
1.740	$0^+; 1$	1	1.58	1.42	2.6
2.155	$1^+; 0$	1	0.52	0.41	0.71
3.590	$2^+; 0$	1	0.28	0.10	0.30
4.773	$3^+; 0$				0.15
5.112	$2^-; 0$	2	$\leqslant 0.27$		
5.166	$2^+; 1$	1	$\leqslant 1.85$ [e]	0.43	
5.180	$1^+; 0$	1	$\leqslant 3.14$ [e]		
5.924	$2^+; 0$	1	0.48	0.49	1.2
6.025	4^+				
6.133	3^-	2	0.24		
6.561	(2^+)	(1, 2)	(1.61, 0.17)		
7.002	$(1, 2)^+; (0)$	1	(0.59, 0.35)		
7.431	$(1)^-; 0+1$				
7.467	1^+				
7.477	$2^-; 1$				
7.559	$0^+; 1$				
7.84	1^-	2	0.28		
8.889	$3^{(-)}; (1)$	2	$\leqslant 0.11$		
8.894	$2^+; 1$	1	$\leqslant 1.45$		

A normalization factor $N = 22.6$ was used (see text).

[a]) Excitation energies and spins and parities are obtained from ref. [12]).

[b]) For $l = 1$ and $l = 2$, respectively, $1p_{3/2}$ and $1d_{5/2}$ transfer are assumed.

[c]) Average of values obtained at $E_d = 12.0$, 15.0 and 16.0 MeV by Park *et al.* [2]).

[d]) Obtained from ref. [21]).

[e]) If the total cross section is due to one component only.

TABLE 3

Spectroscopic information for the $^{9}Be(\alpha, ^3He)^{10}Be$ reaction as obtained from DWBA analysis

E_x [a] (MeV)	J^π [a]	l_n [b]	$S(\alpha, ^3He)$	$S(d, p)$ [c]
0.0	0^+	1	1.58	2.1
3.368	2^+	1	0.38	0.23
5.958	2^+	1	$\leqslant 0.73$	$\leqslant 1.0$
5.960	1^-	2	$\leqslant 0.14$	
6.263	2^-	2	0.08	0.065
7.371	3^-	2	0.26	0.53 [d])
7.542	2^+	1	0.34	
9.27	(4^-)	2	$\leqslant 0.18$	0.2 [d])
(9.4)	(2^+)	1		
11.86	?	2		

A normalization factor $N = 22.6$ was used (see text).

[a]) Excitation energies and spins and parities are obtained from ref. [12]).

[b]) For $l = 1$ and $l = 2$, respectively, $1p_{3/2}$ and $1d_{5/2}$ transfer are assumed.

[c]) Obtained from ref. [22]).

[d]) Calculated utilizing Vincent and Fortune formalism [23]) for unbound states.

full CRC calculations and experimental data for the 3^+ g.s. of ^{10}B as will be discussed in the next section.

The absolute spectroscopic factors were obtained from the above analysis assuming $1p_{\frac{3}{2}}$ and $1d_{\frac{5}{2}}$ for $l = 1$ and 2, respectively. These are listed in tables 2 and 3 for ^{10}B and ^{10}Be, respectively. Relative spectroscopic factors obtained from other reactions are also listed. Because of the strong coupled-channels effects, to be discussed in sect. 4, the spectroscopic information obtained from the DWBA calculations has to be taken with some caution.

4. Coupled-channels analysis of the low-lying states

^{9}Be and ^{10}B are situated in the middle of the 1p shell and thus are expected to be well deformed. In fact, ^{9}Be is known [12]) to have a rotational band ($K^\pi = \frac{3}{2}^-$) built on its ground state. Recently, Kurath [13]) calculated the spectrum of ^{10}B in an *LS* representation in an attempt to understand the electromagnetic transitions in ^{10}B. The spectrum so-obtained for the lowest excited states in ^{10}B (fig. 9) could be divided

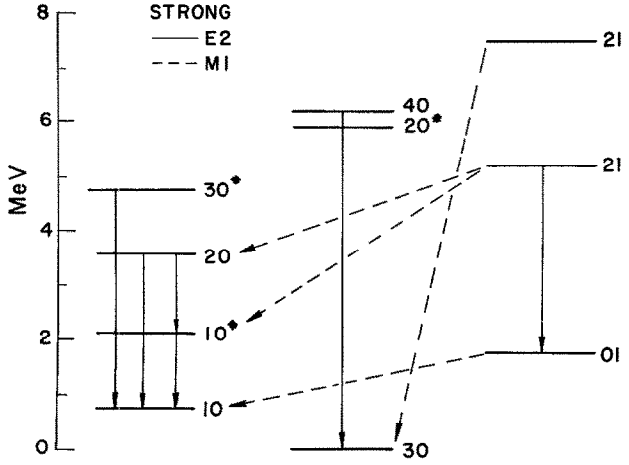

Fig. 9. Band structure in ^{10}B as predicted by Kurath [13]). Solid and broken arrows represent strong E2 and M1 transitions, respectively. States are labelled by (JT).

into three collective bands, belonging to the same [42] *LS* representation. These collective bands with band heads $[(J^\pi T)]$ (3^+0) ground state, (1^+0) at $E_x = 0.72$ MeV and (0^+1) at $E_x = 1.74$ MeV, respectively, have rather weak cross band E2 transitions.

It is obvious that in such deformed nuclei, multistep processes could play an important role in modifying transition strengths for particle transfer. In fig. 10 we show the coupled-channels schemes for which calculations were performed. Since there are no strong E2 cross band transitions, one can perform calculations where

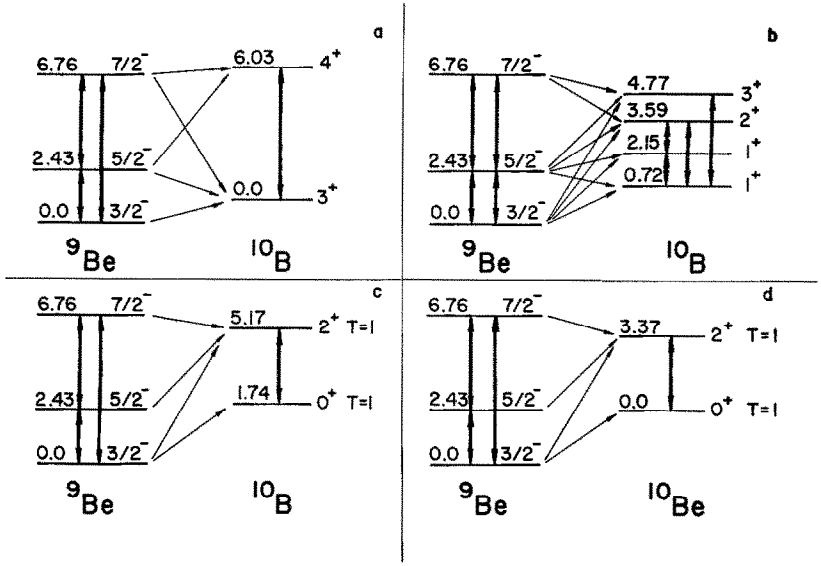

Fig. 10. Schemes for CRC calculations as described in the text. Thin arrows represent one-way single-particle transitions from ^{9}Be to ^{10}B and ^{10}Be. Heavy arrows with two arrow heads indicate strong E2 transitions taken into account in the CRC calculation. Reorientation terms (not indicated) were also included in the CRC calculations. Band structure assumed as suggested by Kurath [ref. [13])]. See caption of fig. 9.

only states of the same band in ^{10}B or ^{10}Be, respectively, are coupled to each other and in turn are coupled by single-particle transfer to states in ^{9}Be. All coupling terms considered in these calculations are represented by lines in fig. 10. Thin lines with one arrow head indicate one-way coupling for single-particle transfer. Thick lines with two arrow heads represent couplings within the collective bands with two-way coupling. Within the collective bands, calculations were performed in the limit of the symmetric rotational model. Coulomb excitation and reorientation terms were included [14]) and only $\lambda = 2$ terms were considered. Wave functions of the transferred single particles were generated in a Woods-Saxon potential, whose geometrical parameters are given in table 1 and whose depth was varied to give the correct separation energies of the transferred particles.

Initial values for the spectroscopic factors for all indicated transitions were obtained from a shell-model calculation performed by Cohen and Kurath [15]). The spectrocopic factors for the two lowest ($1^{+}0$) and ($2^{+}0$) states already included in them the changes due to the modifications of the wave functions of these states as suggested by Warburton *et al.* [16]). These modifications were found [16]) necessary to obtain a better agreement between the theoretical and experimental radiative transition rates for these states. The spectroscopic factors for single-particle transfer connecting the $\frac{3}{2}^{-}$ ground state of ^{9}Be and the following states in ^{10}B: 3^{+} ground state, 1^{+} state at 0.72 MeV, 0^{+} state at 1.74 MeV, 1^{+} at 2.15 MeV and 2^{+} at 3.59 MeV, were further modified so that

DWBA cross sections obtained with these modified spectroscopic factors could reproduce the absolute differential cross sections from the ^{9}Be(^{3}He, d)^{10}B reaction measured by Wegner and Hall [17]) at $E_{^{3}He} = 25$ MeV. This is justified because it was observed that coupled-channels calculations performed for the (^{3}He, d) reaction did not modify the cross sections for these states from those predicted by the DWBA.

TABLE 4

Spectroscopic amplitudes used in the CRC calculations for the low-lying states of ^{10}B

Transition $J_i^\pi \to J_f^\pi, T$	$\sqrt{C^2S}$ [b])	
	$p_{3/2}$ transfer	$p_{1/2}$ transfer
$\frac{3}{2}^- \to 3_1^+, 0$	+0.693 [c]) (+0.775) [d])	
$\frac{5}{2}^- \to 3_1^+, 0$	−0.653	+0.169
$\frac{7}{2}^- \to 3_1^+, 0$	+0.876	
$\frac{5}{2}^- \to 4^+, 0$	+0.493	
$\frac{7}{2}^- \to 4^+, 0$	−0.476	+0.618
$\frac{3}{2}^- \to 1_1^+, 0$	−0.702 [c]) (−0.647) [d])	+0.644 [c]) (+0.591) [d])
$\frac{5}{2}^- \to 1_1^+, 0$	−0.249	
$\frac{3}{2}^- \to 1_2^+, 0$	+0.396 [c]) (+0.409) [d])	+0.311 [c]) (+0.319) [d])
$\frac{5}{2}^- \to 1_2^+, 0$	+0.493	
$\frac{3}{2}^- \to 2^+, 0$		+0.271 [c]) (+0.558) [d])
$\frac{5}{2}^- \to 2^+, 0$	+0.076	+0.196
$\frac{7}{2}^- \to 2^+, 0$	+0.342	
$\frac{3}{2}^- \to 3_2^+, 0$	−0.076	
$\frac{5}{2}^- \to 3_2^+, 0$	−0.529	+0.431
$\frac{7}{2}^- \to 3_2^+, 0$	−0.556	+0.489
$\frac{3}{2}^- \to 0^+, 1$ [a])	−1.116 [c]) (−1.086) [d])	
$\frac{3}{2}^- \to 2^+, 1$ [a])	−0.156	+0.338
$\frac{5}{2}^- \to 2^+, 1$ [a])	−0.773	−0.156
$\frac{7}{2}^- \to 2^+, 1$ [a])	−0.547	

[a]) For the transition to the 0^+ and 2^+ states of ^{10}Be, these spectroscopic factors should be further multiplied by a factor $\sqrt{2}$ because of the isospin Clebsch-Gordan coefficient.

[b]) D. Kurath, private communication. The spectroscopic factors for the (1^+0) and (2^+0) states already include the changes due to modifications of the wave functions of these states by Warburton *et al.* [16]).

[c]) Modified (see text); used in the full CRC calculation.

[d]) Origingal Cohen-Kurath's spectroscopic amplitudes [see also [b])].

This will be discussed further below. In table 4, the final spectroscopic amplitudes as used in the full CRC calculations are listed. Also listed are Cohen-Kurath's spectroscopic amplitudes for those states whose spectroscopic factors had to be modified to fit the ^{9}Be(^{3}He, d) differential cross sections.

The deformation parameters β were obtained from the experimental [12]) B(E2) values by scaling the βR values relative to the βR obtained for the lowest $\frac{3}{2}^- \to \frac{5}{2}^-$,

E2 transition in ^{9}Be such that:

$$B(\mathrm{E2}, I \rightarrow I') \sim \langle I2K0|I'K\rangle^2(\beta R)^2,$$

where R is the real radius of the optical potential of the ($\alpha + {}^{9}$Be) or (t + ^{10}B) channels. The deformation parameter β of the $\frac{3}{2}^- \rightarrow \frac{5}{2}^-$ transition in ^{9}Be was obtained from a χ^2-fit to the ^{9}Be(α, α')^{9}Be inelastic scattering data of the $\frac{3}{2}^-$, $\frac{5}{2}^-$ and $\frac{7}{2}^-$ rotational band in ^{9}Be with calculations performed with the program ECIS [18]) in the limit of the symmetric rotor. In these calculations the parameters of pot. A65 (table 1) were used as starting values. The geometrical parameters of this potential were kept fixed in the χ^2 search, while the imaginary and real well depths were varied along with the deformation parameters β so that a good fit is obtained to the data. Such a fit along with results from an optical-model fit to the elastic scattering cross sections and DWBA predictions to the $\frac{5}{2}^-$ and $\frac{7}{2}^-$ states are shown in fig. 6. It is obvious that the CC results give a better fit to the data of the $\frac{5}{2}^-$ and $\frac{7}{2}^-$ states than the DWBA results. However, the fit to the elastic scattering cross section is inferior to the optical-model fir with pot. A65. The newly determined potential, which will be used in further CRC calculations, is listed as (pot. A65′) in table 1. Moreover, all the deformation parameters β obtained by the scaling procedure described above are listed in table 5.

TABLE 5

Deformation parameters used in the CRC calculations for the low-lying states of ^{9}Be and ^{10}B

Transition $J_i^\pi \rightarrow J_f^\pi$	β	
	(α, t)	(^{3}He, d)
$\frac{3}{2}^- \rightarrow \frac{5}{2}^-$ [a])	0.52	0.64
$\frac{3}{2}^- \rightarrow \frac{7}{2}^-$ [a])	0.50	0.63
$\frac{5}{2}^- \rightarrow \frac{7}{2}^-$ [a])	0.50	0.63
$3_1^+ \rightarrow 4^+$ [b])	0.45	0.66
$1_1^+ \rightarrow 1_2^+$ [c])	0.70	1.03
$1_1^+ \rightarrow 2^+$ [c])	0.46	0.68
$1_2^+ \rightarrow 2^+$ [c])	0.43	0.64
$1_1^+ \rightarrow 3_2^+$ [c])	0.87	1.29
$0^+, T = 1 \rightarrow 2^+, T = 1$ [d])	0.43	0.63

[a]) $K^\pi = \frac{3}{2}^-$ is assumed in the calculations.
[b]) $K^\pi = 3^+$ is assumed in the calculations.
[c]) $K^\pi = 1^+$ is assumed in the calculations.
[d]) $K^\pi = 0^+$ is assumed in the calculations.

It is remarkable to note the large decrease in the β_2 values of the $\frac{3}{2}^- \rightarrow \frac{5}{2}^-$ and $\frac{3}{2}^- \rightarrow \frac{7}{2}^-$ transitions from the values obtained from the DWBA analysis.

All the following CRC calculations were performed with the program CHUCK [19]). The t and ^{3}He potential used in the CRC calculation for (α, t) and (α, ^{3}He) reactions is the same as the one used for DWBA (pot. C in table 1) with the exception that the

imaginary depth was reduced to -14.5 MeV. This was found to give a better fit to the 3^+ g.s. angular distribution as will be described below. In principle the depth of the real potential can also change from the optical-model value when including some of the strongly coupled states as was found in the (^{9}Be+α) channel. However, in the case of the (t+^{10}B) channel it was not possible to perform a χ^2 search for the best optical-potential parameters as was done for the (^{9}Be+α) channel, since no elastic and inelastic scattering cross sections for the (t+^{10}B) channel at the desired energy were available to us.

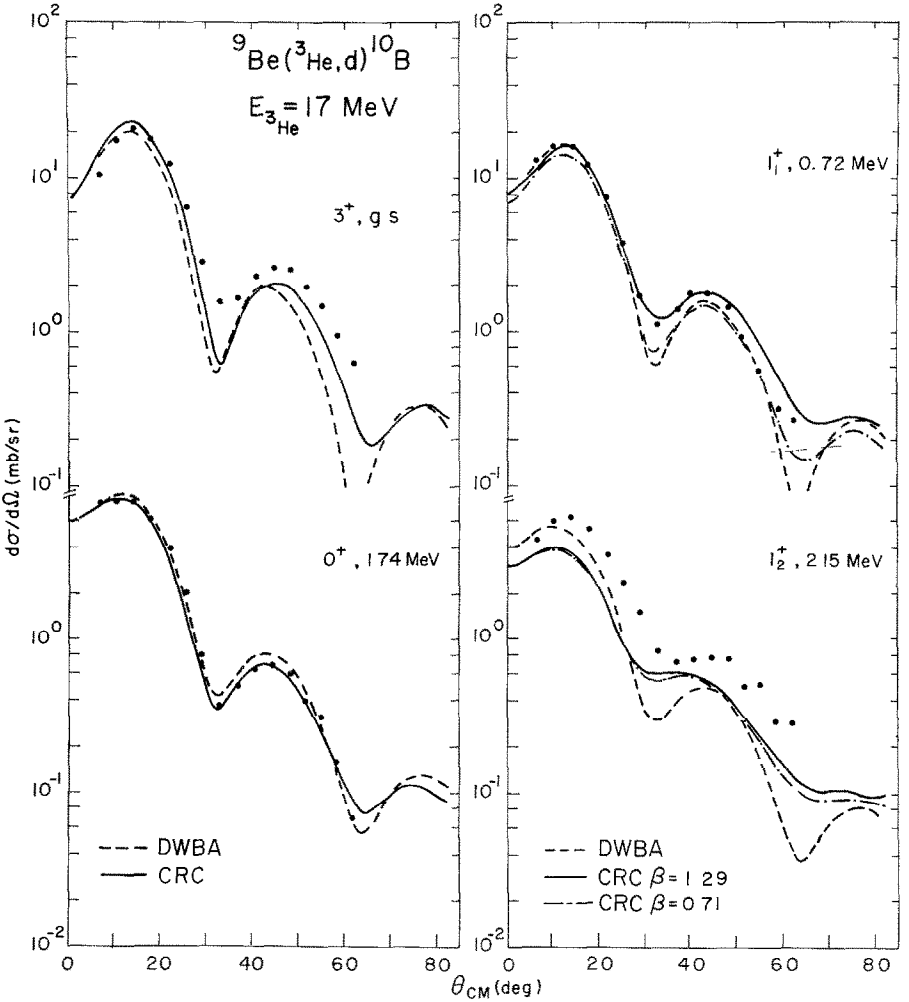

Fig. 11. Differential cross sections of the low-lying states in ^{10}B measured [1]) in ^{9}Be(^{3}He, d)^{10}B at $E_{^{3}He}$ = 17 MeV. Dashed curves are the results of DWBA calculations with a modified set of Cohen and Kurath [15]) spectroscopic amplitudes. Solid and dashed-dotted curves are the results of CRC calculations using the same spectroscopic amplitudes but for values of deformation parameter β_2 connecting the 1_1^+ and 3_2^+ states of 1.29 and 0.71, respectively. See text for more detail.

CRC calculations for the lowest 3_1^+, 1_1^+, 1_2^+ and 0_1^+ states in ^{10}B excited in the (^{3}He, d) reaction at $E_d = 17$ MeV were performed with the coupling schemes a, b and c, respectively. The ^{3}He and deuteron optical potentials used for these and also for DWBA calculations were the same and are listed in table 1. Here again no attempt was made to modify the ^{3}He or deuteron potentials (in table 1, potentials D and E, respectively) for the ^{9}Be(^{3}He, d)^{10}B reaction to account for the strong coupling to the inelastic channels in either the (^{9}Be + ^{3}He) or the (d + ^{10}B) channel, since no elastic and inelastic data in either channel were available to us. The deformation parameters used in these calculations were obtained by βR scaling as described above. These are listed in table 5. A ($S^{\frac{1}{2}}D_0$) factor for the (^{3}He, d) of -225 was used in CHUCK [19]) corresponding to the usual normalization factor $N = 5.06$ in DWUCK [11]). Moreover, a finite-range parameter of 0.77 was used for the (^{3}He, d) reaction.

The results of the CRC calculations for the ^{9}Be(^{3}He, d)^{10}B reaction are shown as solid curves in fig. 11. The dashed curves are the results of DWBA calculations with the same optical potential and spectroscopic factors as used in the CRC calculations. It is evident that the CRC calculations fit the shape of the experimental angular distributions † to the 3_1^+ and 1_1^+ states obtained by Siemssen *et al.* [1]) better than the DWBA calculations. However, the absolute cross sections at the first maxima for the 3_1^+, 1_1^+ and 0_1^+ states hardly change from the DWBA to the full CRC calculation, except perhaps slightly for the 3^+ state. This is not the case, however, for the 1_2^+ state where the CRC predicted cross section is lower by about 30 % than the DWBA predicted cross section. Since these results indicate that in the ^{9}Be(^{3}He, d) reaction, coupled-channel effects are minimal, at least for the lowest 3^+, 1^+ and 0^+ states, we performed also DWBA calculations for ^{9}Be(^{3}He, d) to the low-lying 3_1^+, 1_1^+, 0_1^+, 1_2^+ and 2^+ states, for a ^{3}He bombarding energy of 25 MeV. The optical-potential parameters used for these calculations are those of table 3, they are the same that were used previously. The $p_{\frac{1}{2}}$ and $p_{\frac{3}{2}}$ amplitudes obtained from the shell-model calculation of Cohen and Kurath [15]) were used. These amplitudes were multiplied for each state by the same scaling factor so that the theoretical DWBA curves so-obtained were normalized to the first maxima of the absolute differential cross reactions obtained [13]) for these states in the ^{9}Be(^{3}He, d) reaction at $E_{^3\mathrm{He}} = 25$ MeV. They are listed in table 4 and are used for the CRC calculation for the (^{3}He, d) and the (α, t) reaction.

Having determined spectroscopic factors from fits to the (^{3}He, d) data as described above, full CRC calculations in zero range were performed for ^{9}Be(α, t)^{10}B and ^{9}Be(α, ^{3}He)^{10}Be with the coupling schemes a, b, c and d shown in fig. 10. A finite-range factor of 0.70 was used for the (α, t) and the (α, ^{3}He) reactions. The deformation parameters used were those of table 5. The alpha and triton (^{3}He) optical potentials

† The cross sections for the 3_1^+, 1_1^+, 0_1^+ and 1_2^+ given by Siemssen *et al.* [1]) were given in arbitrary units. The CRC predicted cross sections are in absolute units (mb/sr) and they seem to fit the data of Siemssen *et al.* [1]) if the arbitrary units are taken as mb/sr.

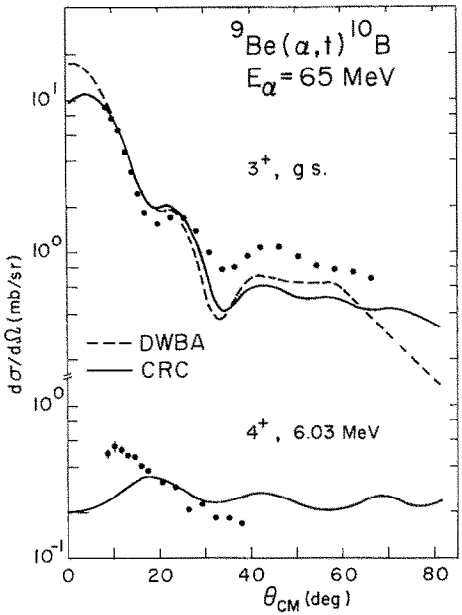

Fig. 12a. $^{9}Be(\alpha, t)^{10}B$ cross sections to the 3^+, g.s. and 4^+, 6.03 MeV state in ^{10}B. Dashed and solid curves are the results of DWBA and CRC calculations described in more detail in the text.

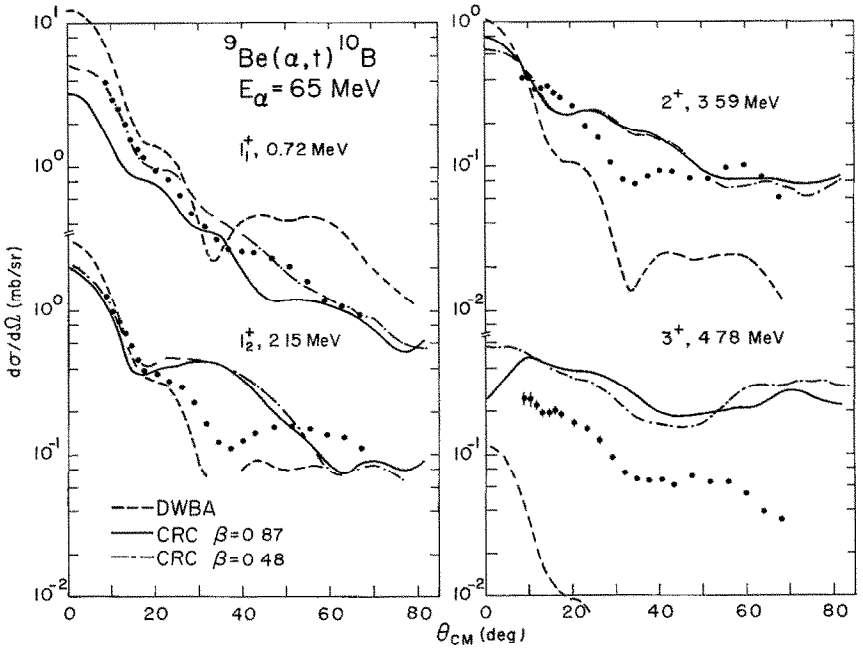

Fig. 12b. $^{9}Be(\alpha, t)^{10}B$ cross sections to the members of the band suggested by scheme b of fig. 10. CRC calculations are performed for two values of β_2 connecting 1_1^+ and 3^+, 4.78 MeV states: $\beta_2 = 0.87$ (solid curves) and $\beta_2 = 0.48$ (dashed-dotted curves). Dashed curves are the results of DWBA calculations.

used for these CRC calculations are (A65′) and C, respectively. A $(S^{\frac{1}{2}}D_0)$ of 476 for the (α, t) and (α, ^{3}He) reactions was used in CHUCK corresponding to a normalization factor $N = 22.6$ in DWUCK. This was found necessary to obtain good agreement between the full CRC predicted differential cross section, with the spectroscopic amplitudes as modified by the (^{3}He, d) reaction analysis, and the experimental differential cross section for the 3^+ g.s. of ^{10}B. This normalization factor is in rather good agreement with the value obtained recently by Brugge *et al.* [20]) from an analysis of the (^{3}He, α) reaction on ^{48}Ca.

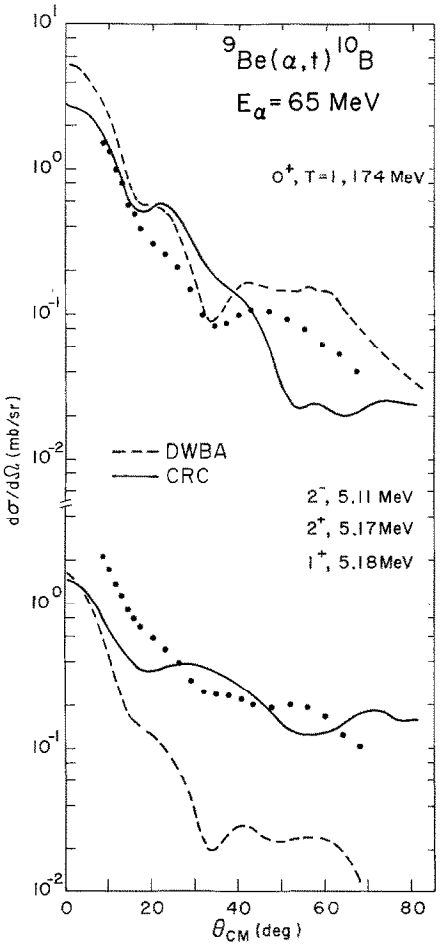

Fig. 12c. ^{9}Be(α, t)^{10}B cross sections to the 0^+, $T = 1$ states at 1.74 MeV and to an unresolved triplet of states at 5.11 MeV (2^-), 5.17 MeV (2^+, $T = 1$) and 5.18 MeV) (1^+). DWBA and CRC calculations are represented by dashed and solid curves, respectively.

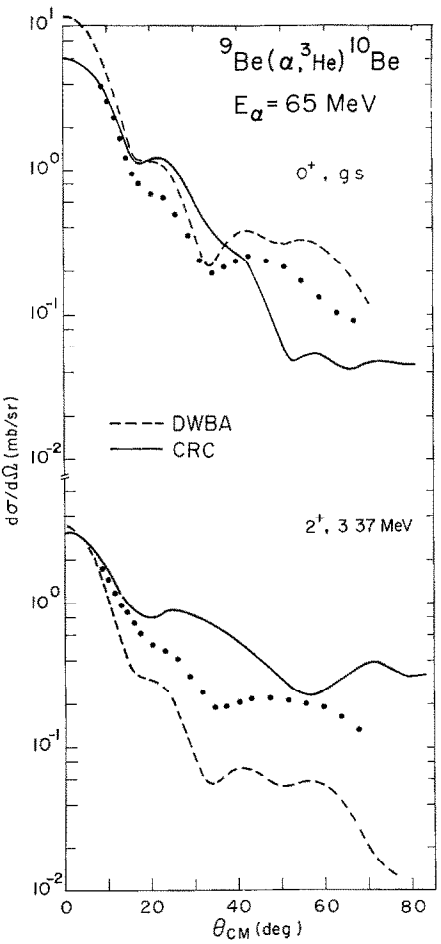

Fig. 12d. ^{9}Be(α, ^{3}He)^{10}Be cross sections to the 0^+ g.s. and 2^+, 3.37 MeV state. CRC calculations using scheme d of fig. 10 are represented by solid curves. Dashed curves represent DWBA calculations.

The results for the full CRC calculations for the coupling schemes a, b, c and d of fig. 10 are shown for all the involved states of ^{10}B and ^{10}Be in figs. 12a, 12b, 12c and 12d, respectively. Here the triton and ^{3}He optical potential used was that of table 1 with the reduced, 14.5 MeV, imaginary depth. The effect of reducing the imaginary depth was found to give a better fit to the 3^+ and 1^+ B(E2) value which is known to be very large. It is in fact three times the value obtained from the adiabatic rotational model [13]), which on the other hand is found [13]) to give a good description of all B(E2) and B(M1) values connecting other states of ^{10}B. For this reason we performed a CRC calculation with the deformation parameter β connecting the 1_1^+ and 3_1^+ states of this band reduced to agree with the adiabatic model prediction. The results of this calculation are shown as dashed-dotted curves in fig. 12b. Excellent agreement is obtained between the predicted and experimental cross sections of the 1_1^+ state. The predicted cross section for the 1_2^+ state is in better agreement with the data in the forward angular region, while the cross section of the 2^+ state remains relatively unchanged and in rather fair agreement with the data. The predicted cross section of the 3^+ state still overestimates the data, but is in rather good agreement with the shape. Obviously, one can obtain a better agreement by varying some of the deformation parameters or spectroscopic amplitudes from the values given by the shell-model calculation of Cohen and Kurath [15]). However, no such attempt was made since the calculations were performed to illustrate the large effects rather than to get a perfect agreement with the data.

We have checked that such a huge change in the β did not deteriorate the good agreement between the DWBA and the CRC calculations for the (^{3}He, d) reaction. The results of the CRC calculation with the reduced β are shown as dashed-dotted curves in fig. 11. They do not differ much from the CRC calculation with the large β.

In figs. 12c and 12d, the experimental and theoretical cross sections to the 0^+ and 2^+, $T = 1$ states in ^{10}B and ^{10}Be, respectively, are shown. It is worth noting that the (α, ^{3}He) and (α, t) transitions to the analog 0^+ states in ^{10}Be and ^{10}B have almost identical angular distributions and differ in cross section by a factor of 2.2. This difference in cross section in the case of complete isospin symmetry of the reaction and vanishing kinematical effects should be equal to 2 (the square of the ratio of isospin Clebsch-Gordon coefficients governing the reaction).

The factor of 2.2 experimentally observed between the 0^+ states of ^{10}Be and ^{10}B is reproduced both in the DWBA and the CRC calculations.

A comparison for the 2^+ states in ^{10}Be and ^{10}B for which the ratio should be again the same, was not possible because the 2^+, $T = 1$ state in ^{10}B was not resolved experimentally from neighbouring 2^- and 1^+, $T = 0$ states. The sum of the cross sections of all these states is displayed in fig 12c. For the 0^+ states, the CRC predicted cross sections seem to agree better with the data than the DWBA predicted cross sections in the forward angular range. However, for the backward angles the DWBA gives a better description of the data. For the 2^+ states, both DWBA and CRC calculations do not give a good fit of the data. Here again no attempt was made to modify the spectroscopic factors of the 2^+ states.

5. Discussion and conclusions

5.1. ELASTIC AND INELASTIC DATA

A curious feature of the optical-model analysis of the present elastic α-scattering data on ^{9}Be at $E_\alpha = 65$ MeV and those of Hauser *et al.* [10]) at $E_\alpha = 104$ MeV, is the tendency for the imaginary part of the optical-model potential to become of shorter range but more diffuse at the nuclear surface at the higher bombarding energy. A χ^2 search for the optical-model parameters that would best fit the detailed and extensive data of Hauser *et al.* [10]) at $E_\alpha = 104$ MeV resulted in a very good fit ($\chi^2 = 2.8$) to the data with optical-model parameters B104 of table 1 with $r_I = 0.636$ fm and $a_I = 1.066$ fm. Using this parameter set and allowing for variations in the real and imaginary depths resulted in a poorer fit (in terms of χ^2) to our elastic α-scattering data at $E_\alpha = 65$ MeV than what could be obtained with regular optical model parameters (A65) with similar geometries for the real and imaginary parts. Such a behaviour of the imaginary part of the optical potential is not unique to this analysis. A short glance at the compilation of ref. [9]) reveals many instances for nuclei $A \leqq 40$, where the imaginary part of the optical potential, for various projectiles and at various energies, has the same behaviour. In some cases, even the real potential reveals a tendency towards shorter range and greater diffuseness. This behaviour is not well understood. It does, however, occur for many nuclei which are well deformed in their ground state. It would be of interest to investigate the problem further and try to understand the reason for such a behaviour.

In our analysis of the inelastic scattering data to the other members of the ground-state rotational band, we used the normal optical-model parameter set A65. A good fit to the data was obtained by a DWBA calculation with a deformation parameter $\beta \simeq 0.68$. A better fit to the inelastic scattering data was obtained with a CC calculation in the framework of the symmetric rotational model. In this calculation both the deformation parameter β and the real and imaginary depths were varied. The goodness of χ^2 fit was judged according to both the elastic and inelastic data. This resulted in optical-model parameters A65′ of table 1, which gave a slightly worse fit to the elastic scattering data. The huge reduction in the depth of the imaginary potential is expected because of the inclusion of the inelastic channels of the g.s. rotational band which seem to account for 50% of the absorption of flux from the entrance channel. This already indicates that transfer reaction channels and other channels are not as important as the inelastic excitation of the $\frac{5}{2}^-$ and $\frac{7}{2}^-$ states of the g.s. rotational band at this α-bombarding energy. The effect of inclusion of just these couplings could affect the transfer cross sections drastically as we will discuss further below.

One of the interesting outcomes of this analysis is that the deformation parameter β needed to fit the inelastic scattering data in the CC analysis is $\beta = 0.52$ and is much smaller than the value obtained from DWBA analysis. This is in contrast with the observation of Votava *et al.* [25]) from their analysis of ^{9}Be(p, p′) at $E_p = 13$

MeV. Moreover, the deformation parameter $\beta = 1.1$ they obtain can in no way be reconciled with our value of $\beta = 0.52$ even if we assume equality of deformation lengths βR to first order. The value they obtain [25]), $\beta R = 2.63$, is much too large if compared to our value of $\beta R = 1.61$. This disagreement between the βR values could be due to the neglect of the imaginary coupling and Coulomb excitation by Votava *et al.* [25]). It is a well known fact that the inclusion of the imaginary coupling increases the calculated cross section and hence reduces the deformation parameter β needed to fit the experimental data.

We have, moreover, studied the predicted cross sections of CC and of DWBA as a function of the deformation parameter β in the framework of the symmetric rotor using complex coupling and including Coulomb excitation. The results could be summarized as follows: (i) while the DWBA cross section varies as β^2, the CC cross section increases as a function β and almost linearly for $\beta > 0.6$; (ii) the CC cross section is larger than the DWBA cross section for the same β, if $\beta \lesssim 0.9$ and becomes smaller for $\beta \gtrsim 0.9$. This last behaviour is slightly different if the coupling to the $\frac{7}{2}^-$ state is dropped. In this case the CC cross section will become smaller than the DWBA cross section for $\beta \gtrsim 1.3$. All the CC calculations were performed with optical-model potential A65′ without any changes.

5.2. TRANSFER DATA: DWBA ANALYSIS

In tables 2 and 3, the spectroscopic factors obtained from our DWBA analysis of the (α, t) and (α, ^{3}He) reactions on ^{9}Be, respectively, are compared with the results obtained from other reactions. Excitation energies and spins and parities are obtained from the compilation of Ajzenberg-Selove and Lauritsen [12]).

A normalization factor of $N = 22.6$ obtained from our CRC analysis was used to obtain the absolute spectroscopic factors of ^{10}B states listed in column 4 of table 1. These spectroscopic factors are to be compared with the relative spectroscopic factors obtained from the (d, n) reaction [2]) and the (^{3}He, d) reaction [21]). It immediately becomes clear that all three sets of spectroscopic factors disagree among each other, especially for the lowest four states which have large spectroscopic factors. The DWBA analysis of the (d, n) and (^{3}He, d) reactions yield a spectroscopic factor for the 1_1^+ state which is almost twice that of the 3^+ g.s. This has already been schematically illustrated in fig. 1. Moreover, the spectroscopic factor for the 0^+, $T = 1$ state as obtained from (^{3}He, d) is again about twice the value obtained from either the (α, t) or the (d, n) reaction. The agreement for the higher states for which spectroscopic factors have been obtained from all three reactions is not much better, e.g. 1^+ state at 2.155 MeV and 2^+ states at 3.59 MeV and 5.924 MeV. The excitation of the 3^+ state at 4.77 MeV is strongly affected by coupled-channel effects which is the reason no spectroscopic factor has been quoted for it from DWBA analysis of our (α, t) data. The 2^+, $T = 1$ state at 5.17 MeV was not resolved from a 2^- state at 5.11 MeV and 1^+ state at 5.18 MeV. Because of the momentum mismatch of the (α, t) reaction

the 2^- state which goes by an $l = 2$ transition would be excited very strongly compared to the 2^+ state which goes by an $l = 1$ transition. This is true even though the spectroscopic factor of the 2^- state could be very small. One can obtain a better upper limit to the 2^- spectroscopic factor in the following way: the ratio of the cross section of the 0^+, $T = 1$ state in ^{10}B to that of the 0^+ g.s. of ^{10}Be is 1/2.2. This is reproduced both in DWBA and CC calculations. The same calculations predict a factor of 1/2.2 for the ratio of the cross section of the 2^+, $T = 1$ state at 5.17 MeV in ^{10}B to the cross section of the 2^+, 1st excited state in ^{10}Be. If this ratio was to be also the experimental ratio which seems to be a reasonable assumption, then we obtain that the spectroscopic factor of the 2^- state at 5.11 MeV in ^{10}B is $\leqq 0.27$. This spectroscopic factor and those for states at $E_x \geqq 6.133$ MeV are new spectroscopic information. However, because of the discrepancies observed between spectroscopic factors obtained for ^{10}B from various reactions at various energies, one should take these spectroscopic factors as well as those of the lower states with some caution. This is due to the strong coupled channels effects observed in these reactions as will be discussed below.

This, of course, also applies for the spectroscopic factors obtained for ^{10}Be from the $(\alpha, {}^3\text{He})$ reaction and which are listed in table 5. These spectroscopic factors disagree with those obtained [22]) from the (d, p) reaction for the lowest two states. For states at $E_x \geqq 7.37$ which are unbound to neutron emission, our analysis was performed differently from that of the (d, p) reaction. While Darden *et al.* [22]) used the method of Vincent and Fortune [23]) for unbound single-particle form factors to obtain their spectroscopic factors, we have assumed in our DWBA analysis that these particles were slightly bound. So observed differences in spectroscopic factors could be due both to coupled-channel effects as well as to the use of different DWBA methods of analysis.

5.3. TRANSFER DATA: CRC ANALYSIS

We have seen in the previous sections that the (d, n) and (^{3}He, d) reactions [2, 21]) if analysed in DWBA result in spectroscopic factors for the 1^+_1, 0.72 MeV state in ^{10}B which are twice the spectroscopic factor obtained for the 3^+, ground state. On the other hand, DWBA analysis of our (α, t) data give about equal spectroscopic factors for both the 1^+_1, 0.72 MeV state and the 3^+ g.s. of ^{10}B. These two states are excited by $l = 1$ transitions for which the (α, t) reaction is badly mismatched. This raises the possibility of two explanations for the discrepancy observed for the spectroscopic factors of the two states in the various reactions. First, because the (α, t) reaction is better matched for $l = 3$ transitions than $l = 1$ transitions, while for the (d, n) and (^{3}He, d) reactions the reverse is true, any f-state admixtures in the 3^+ g.s. of ^{10}B could explain this discrepancy. However, investigation of the pure $l = 1$, DWBA prediction for the differential cross section of the 3^+ and 1^+_1 states (fig. 7), shows that this deviates from the experimental angular distribution of the

1_1^+ state, while for the 3^+ g.s. the DWBA, $l = 1$ transfer gives a rather reasonable description of the experimental angular distribution. Nevertheless, we have performed DWBA calculations with f-state admixtures into the g.s. of ^{10}B. To explain the discrepancy between the spectroscopic factors of the 3^+ g.s. and the 1_1^+, 0.72 MeV state, unreasonable f-state admixtures (of the order of 40–50 %) into the 3^+ g.s. of ^{10}B had to be assumed. This is a much larger admixture than the few percent that one might expect.

The second possibility for explaining this discrepancy is that because of the momentum mismatch of the (α, t) reaction for $l = 1$ transitions, two-step contributions could become significant as compared to one-step $l = 1$ transitions. In this case, constructive interference between one-step and two-step amplitudes enhancing the cross section of the 3^+ g.s., while destructive interference for the 1_1^+ state (or no two-step contributions at all) could result in the observed apparent discrepancy for the stronger excitation of the 3^+ state in the (α, t) reaction.

We have performed many CRC calculations, of which the results (some of which are not shown in any of the figures) could be summarized as follows:

(i) We have performed calculations for the 3^+ g.s., 1_1^+ (0.72 MeV) state and the 0^+, $T = 1$ (1.74 MeV) state, which differ from DWBA calculations only by introducing all couplings between the states of the g.s. band in the ($\alpha + ^{9}$Be) entrance channel. All spectroscopic amplitudes and deformation parameters used in this and all following calculations to be described below are those of tables 4 and 5, respectively. At this stage already, drastic changes in both the shape and the absolute cross sections of the 3^+, 1_1^+ and 0^+ states of ^{10}B were observed. Since no other route could interfere with the direct route, the effect could be explained as changes in the cross sections of these three states due to changes in the distorted waves of the elastic channel because of the strong couplings to the $\frac{5}{2}^-$ and $\frac{7}{2}^-$ state of ^{9}Be. Such an effect has been observed previously by Rehm *et al.* [26]) in their CC analysis of the $^{16}O + ^{40}Ca$ elastic and inelastic scattering data. In our case, the change manifested itself by a large increase in the differential cross section in the region of 15°–45° with a smoothening out of the angular distribution as compared to DWBA predictions.

(ii) Another set of calculations were performed which differ from the DWBA calculations only by introducing the coupling between states of the same collective band in the ($t + ^{10}$B) exit channel. No couplings were taken in the ($\alpha + ^{9}$Be) entrance channel. Here these calculations, while introducing very slight changes in the shape of the angular distributions for the 3^+ and 0^+ states (more drastic changes in the shape of the 1^+ state were observed) decreased the cross sections by factors of 2 or more as compared to DWBA predictions. Large effects were observed for the 1_1^+ state which depended strongly on the value assumed for the deformation parameter connecting the 1_1^+ state to the 3_2^+ state belonging to the same collective band. This could be explained as due to absorption of flux due to couplings to other members of the collective band and/or due to changes introduced into the distorted waves of the exit channel because of these couplings.

(iii) It is apparent from the above that these two types of couplings have opposing effects on the predicted differential cross section of the 3_1^+, 1_1^+ and 0_1^+ states. Therefore, calculations were performed where both of these couplings in the entrance and exit channels and only the direct routes to the 3_1^+, 1_1^+ and 0_1^+ states were included. Indeed, a cancellation between both effects was observed resulting in a predicted differential cross section which is larger or smaller than the DWBA cross section at a certain angle, depending on whether the entrance or exit channel couplings have the dominant effect at that respective angle.

(iv) Including single-particle transfer couplings to the above scheme (iii) thus resulting in the full CRC calculations as described in sect. 4, introduced changes in the differential cross sections of the 3^+, 1_1^+ and 0^+ which were in general smaller than those observed due to couplings in the entrance or exit channels alone. However, the overall changes brought by these couplings tended to improve the shape of the predicted angular distribution in comparison with the experimental angular distribution of the 3_1^+ and 1_1^+ than what was obtained by including both entrance and exit channel couplings alone. Very little changes in shape for the 0^+ state predicted angular distribution was observed. The full CRC calculations gave in general better agreement with the experimental cross sections for the low-lying states of ^{10}B than the DWBA results. There are exceptions, of course, like the 0^+, 1.74 MeV state. However, it is quite possible that variations of some of the parameters could improve the fit to the shape of the 0^+ angular distribution, but this was not attempted. On the other hand, the 1_1^+ cross section could only be reproduced in absolute value by reducing the value of the coupling parameter β between the 1_1^+ and 3_2^+ states to 0.48. An excellent fit was then obtained both in shape and magnitude for the 1_1^+ experimental differential cross section.

(v) The above results already indicate that although the mismatch of the (α, t) reaction for $l = 1$ transfer could play a role in the apparent discrepancy between the spectroscopic factors of the 3_1^+ and 1_1^+ states by enhancing two-step contributions relative to one-step transitions, it is by no means the only contributor to this discrepancy. In fact, we have seen that coupled-channel effects both in entrance and exit channels have very drastic effects on the predicted cross section to the 3_1^+, 1_1^+ and 0_1^+ states. Nevertheless, we have performed DWBA and full CRC calculations in the above schemes for the 3_1^+ and 1_1^+ states where we changed, the Q-value of the (α, t) reaction to make it best matched for an $l = 1$ transition. While the DWBA and CRC calculations for the 3^+ state became almost identical, they differed strongly in the case of the 1_1^+ state. The CRC calculation, though agreeing in shape up to $\sim 40°$ was up to more than a factor of 2 smaller than the DWBA calculation. This indicates the importance of the couplings in the exit channel for the 1_1^+ state, which dominate over all other effects.

(vi) The significance of the full CRC calculations, of course, is its ability to resolve the discrepancy between the strength of excitation of the 3^+ (g.s.) and 1_1^+ (0.72 MeV) state of ^{10}B in (α, t) and the $(^3He, d)$ reactions on ^{9}Be. The same set of Cohen and

Kurath's [15]) spectroscopic amplitudes modified, as discussed previously, to fit in DWBA the ^{9}Be(^{3}He, d) data of Wegner and Hall [17]) gave a globally excellent fit both in shape and magnitude to the differential cross sections of the low-lying states of ^{10}B obtained in both the present (α, t) experiment and the (^{3}He, d) experiment of Siemssen *et al.* [1]). The modification of the spectroscopic amplitudes followed the observation that for (^{3}He, d) DWBA and full CRC calculations agree in magnitude at least at the first maximum. In general, the full CRC calculation gives a better fit to the shape of the (^{3}He, d) angular distribution than does the DWBA. This can be clearly seen for the (^{3}He, d) data of Siemssen *et al.* [1]) at $E_{^{3}\mathrm{He}} = 17$ MeV, displayed in fig. 11.

(vii) This overall agreement in the full CRC calculation goes also for the 0^{+}, $T = 1$ state at 1.74 MeV. Previously, the discrepancy between the (^{3}He, d) and the (d, n) spectroscopic factors for this state was removed by invoking [3,4]) isospin and charge exchange effects in the distorted waves. The same discrepancy exists between the (α, t) and the (^{3}He, d) reaction. However, here the discrepancy was removed by performing full CRC calculations. It is quite possible that the same discrepancy between the (^{3}He, d) and the (d, n) reactions could be due to coupled-channel effects. In fact, such huge CC effects as observed in this study bring to question the role of isospin effects in the entrance and exit channels.

The authors would like to thank D. Kurath for many useful communications and discussions. This work has been performed as part of the research program of the "Stichting voor Fundamenteel Onderzoek der Materie" (FOM) with financial support of the "Stichting voor Zuiver-Wetenschappelijk Onderzoek" (ZWO).

References

1) R. H. Siemssen, G. C. Morrison, B. Zeidman and H. Fuchs, Phys. Rev. Lett. **16** (1966) 1050
2) S. G. Buccino and A. B. Smith, Phys. Lett. **19** (1965) 234;
Y. S. Park, A. Niiler and R. A. Lindgren, Phys. Rev. **C8** (1973) 1557
3) S. Cotanch and D. Robson, Phys. Rev. **C7** (1973) 1714: Nucl. Phys. **A209** (1973) 301
4) K. W. Kemper, S. Cotanch, G. E. Moore, A. W. Obst, R. J. Puigh and R. L. White, Nucl. Phys. **A222** (1974) 173
5) R. H. Siemssen and D. Dehnhard, Phys. Rev. Lett. **19** (1967) 377;
R. J. Puigh, K. W. Kemper, G. E. Moore and R. L. White, Nucl. Phys. **A237** (1975) 1
6) D. Dehnhard and R. H. Siemssen, BAPS **12** (1967) 17;
K. W. Kemper, G. E. Moore, R. J. Puigh and R. L. White, Phys. Rev. **C15** (1977) 1726
7) J. R. Comfort, Program SOFBAL, Internal report KVI-44
8) D. H. Zurstadt, Program OPTIM, University of Colorado, unpublished
9) C. M. Perey and F. G. Perey, Atomic Data and Nucl. Data Tables **17** (1976) 1
10) G. Hauser, R. Löhken, H. Rebel, G. Schatz, G. W. Schweimer and J. Specht, Nucl. Phys. **A128** (1969) 81
11) P. D. Kunz, Program DWUCK, University of Colorado, unpublished
12) F. Ajzenberg-Selove and T. Lauritsen, Nucl. Phys. **A227** (1974) 1
13) D. Kurath, Nucl. Phys. **A317** (1979) 175
14) K. van der Borg, M. N. Harakeh, B. S. Nilsson, Nucl. Phys. **A325** (1979) 31

15) S. Cohen and D. Kurath, Nucl. Phys. **73** (1965) 1;
D. Kurath, private communication
16) E. K. Warburton, J. W. Olness, S. D. Bloom and A. R. Polleti, Phys. Rev. **171** (1968) 1178
17) H. E. Wegner and W. S. Hall, Phys. Rev. **119** (1960) 1654
18) J. Raynal, ECIS, computing as a language of physics (IAEA, Vienna, 1972)
19) P. D. Kunz, CHUCK, University of Colorado, unpublished
20) B. Zeidman, J. L. Yntema and G. R. Satchler, in Proc. Rutherford Jubilee Int. Conf., ed. J. B. Birks (Academic Press, New York, 1961) 515
21) M. A. Crosby and J. C. Legg, Nucl. Phys. **A95** (1967) 639
22) S. E. Darden, G. Murillo and S. Sen, Nucl. Phys. **A266** (1976) 29
23) C. M. Vincent and H. T. Fortune, Phys. Rev. **C2** (1970) 782
24) G. Bruge, M. S. Zisman, A. D. Bacher, R. Schaeffer, C. J. Zeippen and J. M. Loiseaux, Phys. Rev. **C19** (1979) 9
25) H. J. Votava, T. B. Clegg, E. J. Ludwig and W. J. Thompson, Nucl. Phys. **A204** (1973) 529
26) K. E. Rehm, W. Henning, J. R. Erskine and D. G. Kovar, Phys. Rev. Lett. **40** (1978) 1479